Quantifying viral pandemic potential from experimental transmission studies

Elizabeth D. Somsen[1], Kayla M. Septer[2], Cassandra J. Field[2], Devanshi R. Patel[2], Anice C. Lowen [3,4], Troy C. Sutton[2,4], Katia Koelle[4,5]

1 Graduate Program in Population Biology, Ecology, and Evolution, Emory University, Atlanta, GA, USA
2 Department of Veterinary and Biomedical Sciences, The Pennsylvania State University, State College, PA, USA
3 Department of Microbiology and Immunology, Emory University, Atlanta, GA, USA
4 Emory Center of Excellence for Influenza Research and Response (Emory CEIRR), Atlanta GA, USA
5 Department of Biology, Emory University, Atlanta, GA, USA

Abstract

In the past two decades, two pandemic respiratory viruses (H1N1 and SARS-CoV-2) have emerged via spillover from animal reservoirs. In an effort to avert future pandemics, surveillance studies aimed at identifying zoonotic viruses at high risk of spilling over into humans act to monitor the 'viral chatter' at the animal-human interface. These studies are hampered, however, by the diversity of zoonotic viruses and the limited tools available to assess pandemic risk. Methods currently in use include the characterization of candidate viruses using *in vitro* laboratory assays and experimental transmission studies in animal models. However, transmission experiments yield relatively low-resolution outputs that are not immediately translatable to projections of viral dynamics at the level of a host population. To address this gap, we present an analytical framework to extend the use of measurements from experimental transmission studies to generate more quantitative risk assessments. Specifically, we develop modeling approaches for estimating transmission parameters and gauging population-level emergence risk using within-host viral titer data from index and contact animals. To illustrate the use of these approaches, we apply them to two recently published influenza A virus (IAV) ferret transmission experiments: one using influenza A/California/07/2009 (H1N1pdm09) and one using influenza A/Hong Kong/1/1968 (H3N2). We find that, when controlling for viral titers, the H3N2 virus tends to be less transmissible than the H1N1 virus. Because of this difference in infectiousness and more robust replication of H1N1 in ferrets, we further find that the H1N1 virus has a higher projected reproduction number than the H3N2 virus and therefore more likely to cause an epidemic following introduction. Incorporating estimates of the generation interval for each virus, we find that the H1N1 virus has a higher projected epidemic growth rate than the H3N2 virus. The methods we present to assess relative pandemic risk across viral isolates can be used to improve quantitative risk assessment of other emerging viruses of pandemic concern.

Introduction

Pandemics arising via zoonotic spillover from animal reservoirs have resulted in mass human mortality and extreme societal disruption. Notable examples are the 1918 Spanish flu pandemic caused by influenza A virus (IAV) H1N1 and the COVID-19 pandemic caused by SARS-CoV-2. Given the impact of pandemics, there is considerable interest in preventing pathogen emergence, particularly of rapidly spreading respiratory pathogens. One key component in preventing pathogen emergence involves surveillance of reservoir species to identify viruses with pandemic potential. However, reservoir species can harbor diverse viral pathogens, resulting in a large pool of possible pre-pandemic strains. Approaches to winnow down the considerable diversity of candidate viruses to those that are more likely to cause a pandemic are therefore essential to guiding advanced control efforts to mitigate pandemic risk.

One approach for prioritizing viruses for preparedness and control strategies involves genotypic and phenotypic characterization of viral strains to identify those with traits associated with pandemic risk [1, 2]. For example, assays measuring IAV hemagglutinin receptor binding specificity are used to determine if an influenza virus preferentially binds cells with α-2,3 or α-2,6 sialic acid linkages. IAVs with the α-2,3 binding preference generally do not transmit well from person to person. For many relevant traits, however, genotypic characterizations provide only limited information because the relationships between viral genotypes and their phenotypes have not been fully characterized. Risk assessments based on genetic analyses are therefore limited to traits where the genetic basis is well understood.

Experimental transmission studies have also been widely used to estimate the transmission potential of viral strains. For IAV risk assessment, ferrets are often used because of similarities between ferrets and humans in phenotypes relevant to infection and transmission, such as viral attachment [3] and clinical signs. A notable study found evidence for a strong positive correlation between ferret-to-ferret transmission probability (as measured by secondary attack rate) and IAV circulation patterns in humans [4]. The findings of this study were particularly impactful because the investigators used results from numerous ferret experiments in their assessment of the relationship between secondary attack rates and IAV circulation patterns in humans. Results from these types of transmission experiments provide semi-quantitative measurements of transmission potential, one aspect of pandemic risk. However, the read-outs of these experiments are typically low-resolution estimates. For example, in a study with three index-contact pairs, the observed overall transmission efficiency could be 0% (0/3), 33% (1/3), 67% (2/3), or 100% (3/3). Given the cost and effort involved in carrying out these experiments, extracting more information about transmission from these data would be worthwhile. To this end, we here develop new methods to improve risk assessment using measurements commonly taken during experimental transmission studies. We specifically propose to use within-host viral titer data to improve pandemic risk assessment. Our approach relies on the titer data from infected index animals as well as infected contact animals to provide quantitative estimates of transmission parameters and epidemiological components of pandemic risk. We present our approach in the context of two recently performed IAV experimental transmission studies [5], the first using a 2009 pandemic H1N1 strain and the second using a 1968 pandemic H3N2 strain.

Results

Infection rates and viral kinetics in index and contact ferrets

The airborne transmission studies analyzed here have previously been described in detail, and their data have been made publicly available [5]. A brief overview of the study design is provided in the Methods section. In these studies, airborne transmission was assessed from index ferrets to contacts using inoculation doses from 10^0 to 10^6 $TCID_{50}$. We considered an animal to be infected if viral shedding over the limit of detection (10^1 $TCID_{50}$/mL) was observed at any sampled timepoint. Transmission efficiency was defined as the fraction of contact ferrets that were infected by their paired index in the subset of pairs in which the index became infected.

The transmission efficiency for each experiment is listed in Figure 1. For H1N1, it ranges from 75-100%; for H3N2, it ranges from 33-100%. Interestingly, the transmission efficiencies observed for H1N1 all fall within the range of respiratory droplet attack rates that Buhnerkempe and colleagues [4] would predict as having a high probability of a supercritical classification in humans. In contrast, the efficiencies observed in the H3N2 transmission study span a range between subcritical and supercritical classification in humans.

Estimation of the transmission function

Several qualitative patterns emerge from inspection of the viral titer dynamics shown in Figure 1. First, the likelihood of transmission to a contact animal generally appears to decline with decreasing virtual titers in the index. Second, in the H1N1 study, transmission to a contact animal appears to occur earlier at higher inoculum doses. This is likely because higher inoculum doses tend to result in higher viral titers in the index animals shortly following challenge. As such, viral titer levels appear to impact not only *whether* a contact animal gets infected but, in the case of infection, *when* it gets infected. This observation is key to the development of our analytical approach.

Given that the viral kinetics of the index appear to impact the probability and timing of transmission, we here develop a quantitative framework for estimating transmission rates between index and contact animals that depend on index viral titers. We specifically rely on approaches that allow for a time-varying force of infection to quantify how the transmission rate between an index animal and its contact depends on time-varying index viral titers. We define the force of infection λ that an index animal exerts on a contact animal at time t as the product of its log-transformed viral load V (measured in $TCID_{50}$/mL) at time t and a parameter s that quantifies infectiousness:

$$\lambda(t) = s \times log_{10}(V(t)) \tag{1}$$

We use this functional form for the force-of-infection given previous findings, across various viral pathogens, that transmission appears to depend on the log of the index animal's viral titer, rather than its viral titer on a linear scale [6, 7, 8]. The probability that an index transmits to its contact and the timing of the transmission event are both functions of this time-varying force of infection (Methods). Given observed index viral titers (Figure 1) and information on infection times of the contacts, we can statistically estimate the parameter s (Methods). Figure 2A shows the estimates of s derived from the H1N1 and H3N2 transmission studies. For H1N1, the maximum likelihood estimate is $s = 0.114$ (95% confidence interval (CI) = $[0.069, 0.176]$) and for H3N2, it is $s = 0.047$ ($[0.023, 0.082]$). Our estimates for s indicate that the infectiousness of H3N2-infected ferrets tends to be lower than that of H1N1-infected ferrets while controlling for index viral titers. Using our estimates of s, we calculated the probability of a contact becoming infected if exposed for a period of one day to an index animal with a given viral titer

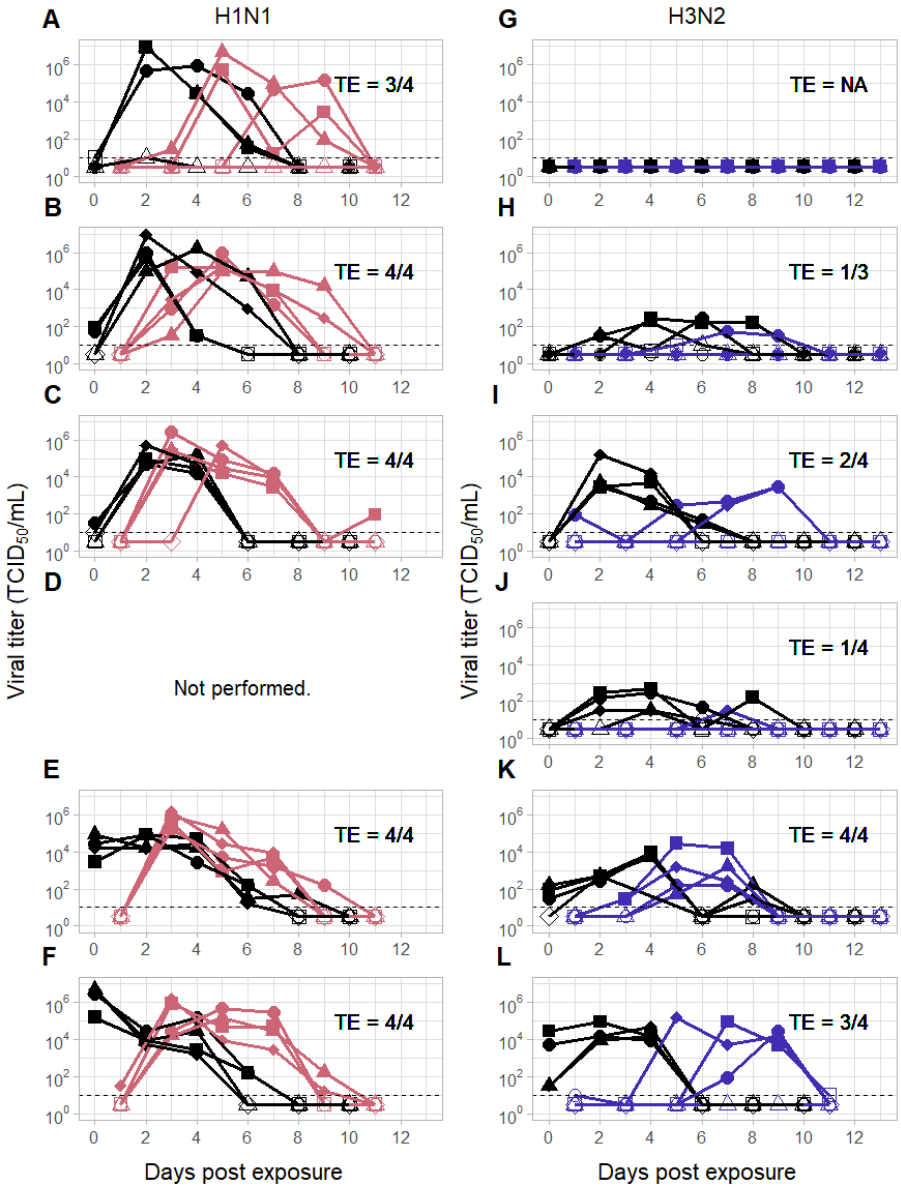

Figure 1. Viral kinetics in the H1N1 and H3N2 experimental transmission studies. The left column shows H1N1 viral kinetics in index ferrets (black) and respiratory contact ferrets (pink). The right column shows H3N2 viral kinetics in index ferrets (black) and respiratory contact ferrets (blue). Rows correspond to different index inoculum doses: (A, G) 10^0, (B, H) 10^1, (C, I) 10^2, (D, J) 10^3, (E, K) 10^4, and (F, L) 10^6 $TCID_{50}$. The limit of detection is shown as a dotted line at 10^1 $TCID_{50}$/mL. Transmission pairs share the same marker. Open markers at $10^{0.5}$ $TCID_{50}$/mL denote samples with viral titers that fall below the limit of detection. Each panel further provides the transmission efficiency (TE) in that experiment, with the denominator denoting the number of infected index animals in the experiment and the numerator denoting the number of contact animals that became infected. NA = Not Applicable. Data are from [5].

(Figure 2B). As expected, given the higher value of s for H1N1 than for H3N2, the probability that a contact becomes infected is higher for H1N1 than for H3N2 at a given

index viral titer.

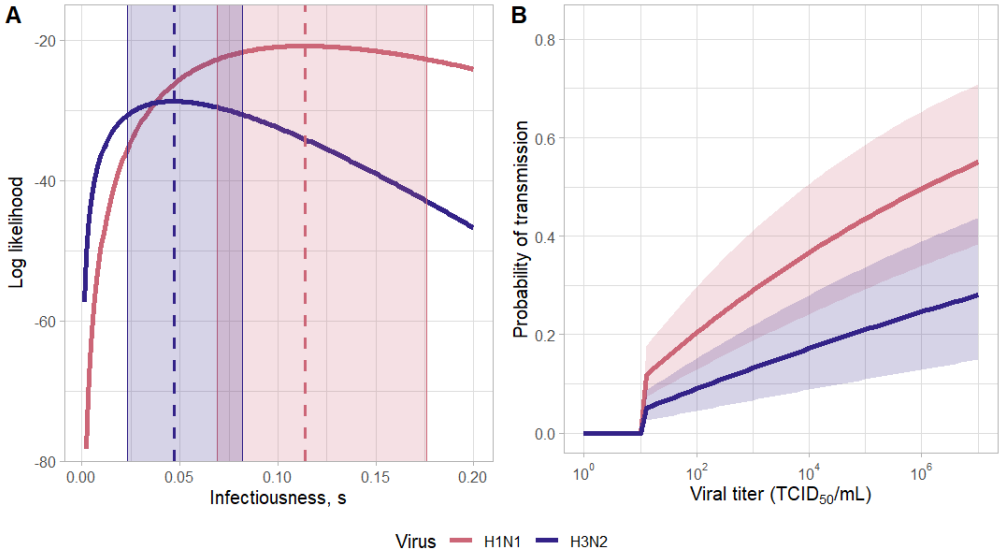

Figure 2. Statistical estimation of the transmission function. (A) The log likelihood profile for the parameter s for both the H1N1 virus (pink) and the H3N2 virus (blue). Dashed lines show the maximum likelihood values of s. Shaded regions show the 95% confidence intervals. (B) Calculated probabilities of transmission to a contact after a one-day exposure to an index animal with a constant viral titer, as given on the x-axis. Solid lines show the probabilities calculated using the maximum likelihood estimates for s. Shaded regions show transmission probabilities that fall within the 95% confidence interval values for s.

Quantification of parameters at the transmission event

Whereas the index animals in these experimental transmission studies received direct intranasal challenge with varying inoculum doses, the contact animals acquired their infections via inhalation of infectious respiratory particles that were shed by the index animals. As such, one could argue that the viral titer dynamics observed in the contact animals are more likely to resemble natural infections. Indeed, a qualitative re-inspection of Figure 1 indicates that, for H1N1, neither the peak viral titer nor the duration of infection in contact animals appears to depend on the index's inoculum dose. Similarly, in the H3N2 study, although there appears to be considerably more heterogeneity across the contact animals in their viral titer dynamics, neither peak viral titers nor infection durations appear to depend systematically on index inoculum doses or their viral kinetics. In both the H1N1 study and the H3N2 study, viral titers in the contact animals appear to start off at low levels, reaching their peaks within 2 to 4 days. Here, to quantify parameters at the transmission event, we therefore assume that the viral titer dynamics observed in the contact animals are representative of those in natural infections.

Our approach to projecting parameters across the transmission event relies on combining viral titer dynamics observed across contact ferrets with our parameterized transmission function. These contact ferrets become "theoretical" index animals, and we use their observed titer dynamics and the transmission function to simulate the expected number of secondary infections (Methods). Figures 3A and 3B show a single stochastic realization of the offspring distribution for H1N1 and H3N2 "theoretical" index

animals, respectively, assuming 15 hour-long contacts per day. (We chose this contact rate based on contact rates previously estimated for children under the age of 18 [9].) By eye, both offspring distributions appear to follow a negative binomial distribution with different means. From our stochastic simulations, we could also keep track of when transmissions occurred from each infected animal and use this information to calculate the time between the infected animal's infection and onward transmission, defined as the generation interval. Figures 3C and 3D show these generation times for the H1N1 and H3N2 secondary infections that were realized and are shown in 3A and 3B, respectively.

To scale up from the single stochastic realizations shown in 3A-D for the populations of H1N1 and H3N2 "theoretical" index ferrets, we performed 1000 stochastic realizations for each virus. For each realization, we fit a negative binomial distribution to the resultant offspring distribution and calculated the mean and the overdispersion parameter k of this distribution. The mean of this distribution is, by definition, equivalent to the reproduction number R_0, estimated empirically from a stochastic realization. Figure 3E plots the distribution of R_0 values that were estimated for the H1N1 and H3N2 viruses using the 1000 stochastic realizations. From this figure, it is clear that the R_0 estimated for the H1N1 virus is substantially higher than the one estimated for the H3N2 virus, even with considerable uncertainty in its exact value (Welch's two sample t-test, $p < 0.001$). Moreover, at the contact rate assumed, the R_0 estimated for the H1N1 virus exceeds one in almost all of the simulations, where it rarely exceeds one for the H3N2 virus. This indicates that, at this contact rate, the H1N1 virus would have pandemic potential whereas the H3N2 virus would not.

Figure 3F shows the cumulative distributions of the overdispersion parameters estimated for the H1N1 and H3N2 viruses from their respective stochastic realizations. For the H1N1 virus, we find that none of the 1000 stochastic simulations have an estimated overdispersion parameter k of less than one. For the H3N2 virus, less than 20% of the simulations have an estimated k of less than one. This indicates that there is relatively little transmission heterogeneity for both the H1N1 and the H3N2 viruses, with transmission heterogeneity being particularly low for the H1N1 virus. Note that, for both the H1N1 and H3N2 viruses, the estimated overdispersion values only capture transmission heterogeneity stemming from interindividual variation in viral titers. As such, our estimates of the extent of transmission heterogeneity will be lower bound estimates. This is because of additional variation that contributes to transmission heterogeneity, such as heterogeneity in contact rates that occur in real world settings.

Finally, we calculated the mean generation interval T_c for the H1N1 virus and for the H3N2 virus from each of the stochastic simulations. The distributions of these mean generation intervals are shown in Figure 3G. We find that the mean generation interval for the H3N2 virus is slightly shorter than for the H1N1 virus, at 3.50 versus 3.79 days (Welch's two sample t-test, $p < 0.001$). However, this difference is unlikely to be biologically significant.

Prediction of pandemic potential and dynamics

Above, we assumed a single contact rate (of 15 hour-long contacts per day) to project the number of secondary infections for each of the two viruses and to estimate their generation intervals. The chosen contact rate impacts the distribution of secondary infections and thus our estimates of R_0. In Figure 4A, we show how our R_0 estimates change for the H1N1 and H3N2 viruses across a broad range of contact rates. The range of contact rates we consider span those deemed relevant for a respiratory virus of humans [9].

We can use the R_0 estimates shown in Figure 4A to predict the risk of pandemic establishment of the two viruses, given an assumed contact rate (Methods). Figure 4B shows this establishment risk for each virus, under two different transmission hetero-

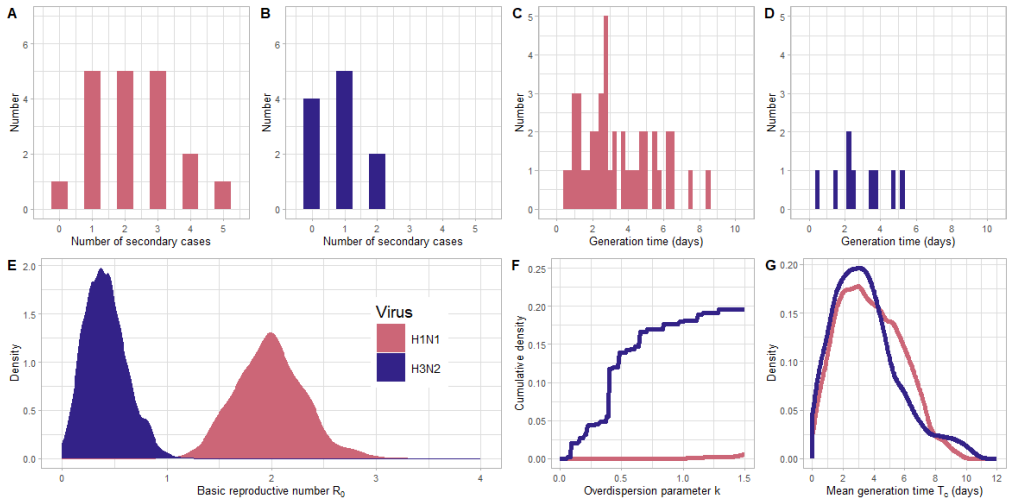

Figure 3. Estimation of transmission event parameters for the H1N1 and H3N2 viruses. (A) Distribution of the number of secondary infections generated by n=19 H1N1 contact animals. (B) Distribution of the number of secondary infections generated by n=11 H3N2 contact animals. In panels (A) and (B), the distributions each show the outcome of one stochastic realization, assuming each animal has 15 one-hour long contacts per day. (C) The generation intervals for each secondary case generated in the H1N1 simulation shown in panel (A). (D) The generation intervals for each secondary case generated in the H3N2 simulation shown in panel (B). (E) The distribution of R_0 values from the 1000 H1N1 and 1000 H3N2 stochastic simulations. (F) The cumulative distribution of overdispersion (k) values from the H1N1 and H3N2 stochastic simulations that resulted in at least one individual transmitting infection. This was 1000 simulations for H1N1 and 989 simulations for H3N2. (G) The distribution of mean generation intervals from the 1000 H1N1 and 1000 H3N2 stochastic simulations.

geneity assumptions: one with no transmission heterogeneity ($k = \infty$) and one with a moderate level of transmission heterogeneity ($k = 1$) that exceeds our simulated expectations (Figure 3F). Across the range of contact rates considered, the R_0 of the H3N2 virus is subcritical (that is, has $R_0 < 1$). As such, regardless of the extent of transmission heterogeneity assumed, the probability of establishment of this virus (in the absence of viral adaptation) is zero. For the H1N1 virus, at contact rates below 8 hour-long contacts per day, the virus is not predicted to establish due to a subcritical basic reproduction number ($R_0 < 1$). The first contact rate at which H1N1 is estimated to have a supercritical basic reproduction number ($R_0 > 1$) is at 8 contacts per day. Increases in daily contact rates above this critical value result in higher probabilities of viral establishment, although the exact probabilities depend on the extent of transmission heterogeneity. As theoretically expected [10], higher levels of transmission heterogeneity lower the probability of viral establishment. In the absence of transmission heterogeneity ($k = \infty$), the probability that the H1N1 virus establishes is approximately 87% when the contact rate is 18 contacts per day, corresponding to the contact rate of the age group with the highest number of daily contacts in the study by Mossong and colleagues [9]. At a contact rate of 7 contacts per day, corresponding to the contact rate of the age group with the lowest number of daily contacts, the probability that the H1N1 virus establishes is 0%.

Previous studies have pointed out that initial R_0 values for a spillover virus matter for projecting pandemic risk, even if they fall below one [11]. This is because viruses have

the potential to adapt as they transmit between individuals along stuttering chains. At R_0 values closer to one, the length of these stuttering chains is expected to be longer than at R_0 values closer to zero, providing viruses with higher R_0 greater opportunity to adapt and thus to ultimately establish. In Figure 4C, we plot for each virus considered, the average length of stuttering chains across the assumed range of contact rates (Methods). We plot these average lengths only for the subset of contact rates for which a virus still has a subcritical (< 1) R_0. At higher contact rates, the average length of stuttering chains is higher. For the H3N2 virus, however, the average length of the stuttering chain stays small, such that one might not expect viral adaptation to readily occur along early transmission chains.

Finally, we can use our estimates of R_0, shown in Figure 4A, along with a specified generation time distribution, to estimate the intrinsic growth rates (r values) of the viruses under various contact rate scenarios. The intrinsic growth rate of a virus is important to project in that it specifies the viral doubling time at the level of the host population and therefore the speed at which a pandemic takes off [12]. Figure 4D shows intrinsic growth rate estimates for both viruses across the range of assumed contact rates, under the assumption of a mean generation time of 3.78 days for H1N1 and 3.49 days for H3N2 (Methods). Because estimates of the intrinsic growth rate are impacted by the shape of the generation interval distribution (not only its mean) [13, 14], we consider two extremes for this distribution's shape: an exponential distribution (where the variance of the distribution is equal to the mean of the distribution) and a delta distribution (where all probability density lies at the mean value). For both viruses, projected intrinsic growth rates are higher at higher contact rates, as expected. For the H1N1 virus, at contact rates that yield supercritical R_0 values, intrinsic growth rates are higher (and doubling times shorter) under the exponential distribution than under the delta distribution, again, as expected. For the H3N2 virus, intrinsic growth rates do not exceed zero, consistent with the R_0 value of this virus falling below one across the range of contact rates considered.

Of note, a previous work estimated the intrinsic growth rate of the 2009 H1N1 virus to be $r = 0.37$ per day during the early phase of its expansion [15], consistent with our results at approximately 18 hour-long contacts per day under exponentially distributed generation times. This is broadly compatible with average human-to-human contact rates quantified in [9].

Discussion

Here, we developed an analytical approach to gauge the pandemic potential of zoonotic viruses using viral titer data from experimental transmission studies. Our approach relied on estimating the parameters of a transmission function using information on index animal viral kinetics and the timing of contact animal infection. It further relied on assuming that the viral kinetics of contact animals reflected those of animals that would be naturally infected with the viruses considered. We applied our approach to existing transmission study datasets that used H1N1 and H3N2 IAV isolates and found that the H1N1 virus had higher pandemic potential than the H3N2 virus (Figure 3).

Before more generally discussing the strengths and limitations of our analytical approach, we first aim to interpret these specific application results. In humans, H3N2 is known to have a higher annual attack rate than H1N1 [16], and as such, our conclusion of higher pandemic potential of the H1N1 virus seems at odds with observed circulation patterns of the seasonal IAV subtypes. There are several possible explanations that could account for this apparent discrepancy. One is simply that ferret models do not accurately recapitulate the difference in human-to-human transmission between these two subtypes. A second is that there are differences in the relative contribution of

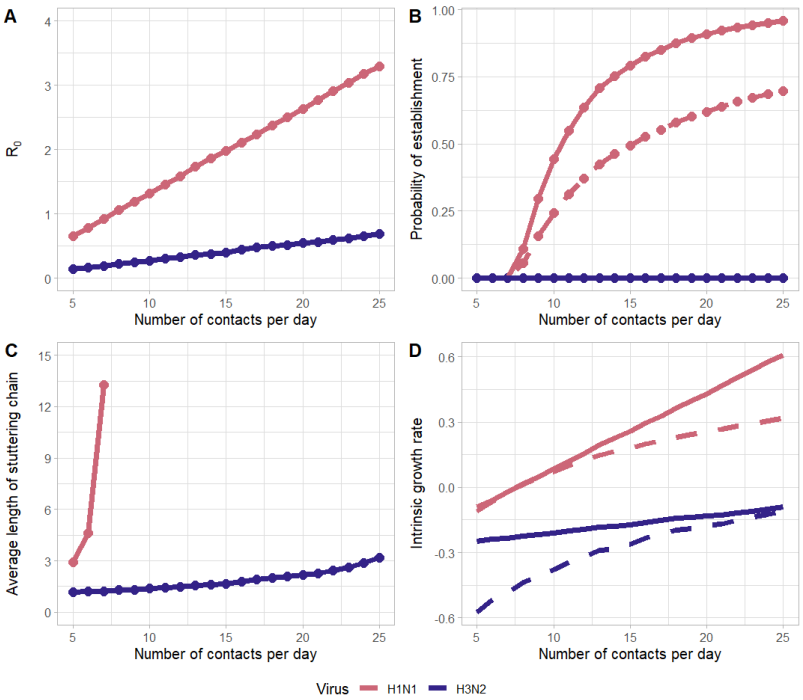

Figure 4. Prediction of pandemic potential and dynamics. (A) Estimates of the reproduction number R_0 for the H1N1 and H3N2 viruses across a range of contact rates. (B) The probability of pandemic establishment for the H1N1 and H3N2 viruses across a range of contact rates. The solid line indicates probabilities in the absence of transmission heterogeneity ($k = \infty$). The dashed line indicates probabilities with a moderate level of transmission heterogeneity ($k = 1$). (C) The average length of stuttering transmission chains across a range of contact rates for both viruses. (D) Estimated intrinsic growth rates (per day) of the H1N1 virus and the H3N2 virus across a range of contact rates, assuming both an exponential (solid lines) and delta (dashed lines) distribution of generation intervals. The doubling time of an epidemic decreases as r increases. When $r = 0.07$, the doubling time is 10 days; when $r = 0.14$, the doubling time is 5 days; and when $r = 0.35$, the doubling time is 2 days. In all panels, H1N1 virus projections are shown in pink and H3N2 virus projections are shown in blue.

transmission modes. For example, if direct contact transmission plays a larger role in driving human transmission of H3N2 than H1N1, these experiments would not capture these differences. A third is that H3N2 is not intrinsically more transmissible than H1N1 in humans, but rather that H3N2 antibodies decay more rapidly than H1N1 antibodies. This possibility is supported by a human cohort study that found that antibodies for a seasonal H3N2 virus (H3N2Pe09) decayed more rapidly than those for H1N1pdm09 [17]. This would make H3N2 reinfections more likely and therefore annual attack higher for H3N2 than for H1N1, despite a possibly lower H3N2 basic reproduction number. A fourth possible explanation is that H3N2 is dominant over H1N1 in its seasonal circulation because it has been circulating in humans for longer and has accumulated adaptive mutations that promote its transmission. The viruses used in this study were generated by reverse genetics and minimally passaged, and so represent isolates from early during their respective pandemics (1968 for H3N2 and 2009 for H1N1), so these isolates would not include subsequent adaptive substitutions that have accrued since their time of emergence. A final possibility is that the H3N2 virus used to challenge index animals

acquired substitutions during laboratory culture that attenuated its transmission in ferrets. The A/Hong Kong/1/1968 stock was passaged three times in monkey cells and three times in eggs prior to plaque purification [5]. Substitutions that occurred during this process could therefore explain the apparent discrepancy between the transmission of this virus in humans, where it apparently transmitted efficiently and caused a pandemic, and in ferrets, where it transmits poorly if index animals are challenged at low inoculum doses.

We now turn to discussing some of the benefits that come with the analytical approach we presented here. In addition to being able to assess relative pandemic potential of different viral strains, our approach provides insight into why one virus might have higher transmission potential than another. For example, we found that our estimate of the transmissibility parameter s was slightly higher for H1N1 than it was for H3N2 (Figure 2). This indicates that an individual infected with H1N1 at a given viral titer is more likely to transmit to a contact than an individual infected with H3N2 at the same viral titer. However, it seems likely that the primary reason that H1N1 had a higher transmission potential than H3N2 was because viral titers were higher in H1N1-infected animals than in H3N2-infected animals (Figure 1). Mutations which increased viral titers in H3N2 infected individuals to the level of H1N1 would close the gap in transmission potential between these viruses. In contrast, if the primary reason for H1N1 having higher transmission potential than H3N2 was due to higher infectiousness (higher s), then one might expect that mutations that result in higher infectiousness might be selected for in zoonotic H3N2 viral populations. Our approach therefore has the potential to help disentangle factors contributing to pandemic potential. An interesting application of this ability would be to consider viral strains differing by a handful of mutations, for example an early pandemic strain and one that carries adaptive mutations from circulation in humans for some relatively short period of time. With data from these types of experimental transmission studies, one could identify whether the observed mutations increased infectiousness (that is, increased s) or simply increased viral titers that would impact downstream transmission.

We aim to use experimental transmission studies in animal models to assess relative pandemic risk in humans. There are several intrinsic limitations associated with this goal, independent of the specifics of the analytical approach. Most obviously, ferrets are not humans. Results based on transmission experiments in ferrets are only relevant to assessing pandemic risk for humans if transmission potential in ferrets reflects transmission potential in humans. One way to circumvent this is to analyze experimental transmission studies in humans [18]. However, the number of transmissions will be severely limited in the case of human studies, such that it is unlikely that transmission parameters could be estimated with confidence. Moreover, to estimate parameters of the transmission function, there needs to be sufficient variation in viral kinetics across index animals and in the timing of infection in the index animals. The dataset we used here ensured substantial variation in index viral kinetics by modulating inoculum dose [5]. Human challenge studies are typically small and, although viral dynamics in challenged individuals may be variable due to diverse influenza exposure histories and other genetic and physiological differences, the variation observed will likely not match that from dose-varying experiments. Additionally, it is unethical to test transmission of emerging viruses in humans because of possible adverse events and side effects. As such, experimental transmission studies in model animals such as ferrets remain the most promising for assessing pandemic risk in humans. Despite the limitations associated with ferrets as a model system, previous analyses do indicate that human infection risk is positively associated with secondary attack rates in ferrets [4], mitigating some of the concern that transmission potential in ferrets does not correlate with transmission potential in humans.

Experimental transmission studies are additionally limited by sampling limitations. In transmission studies like those analyzed here, nasal washes or swabs are often taken from a ferret every or every other day. Viral titers between these measured time points are then inferred through interpolation between the available data points. The viral titers we use to estimate infectiousness therefore do not fully capture the entirety of viral population dynamics in infected hosts. For example, it is unlikely that the time of peak viral titer in an animal coincides with the time that a sample is taken from that animal. Our method is therefore likely to systematically overestimate infectiousness (s), as our interpolations miss the viral peaks. Sampling intervals also affect when we can say that transmission from index to contact has occurred. If sampling was performed more frequently, times of transmission would be more finely resolved.

A second limitation is that our approach assumes that transmission potential is related to viral titer levels in an index, as measured by nasal wash. If transmission potential depended more strongly on viral titers in other locations, our results of relative pandemic risk could be biased. However, several studies using genetically modified viruses have shown that H1N1 and H3N2 viruses transmitted through the air predominately originate from the upper respiratory tract, particularly the nasal respiratory epithelium [19]. Thus, we feel confident that the titer measurements we used to estimate the transmission function are taken from biologically relevant locations in the ferret respiratory tract.

There are several further limitations to our approach that should be discussed. First, we assumed a specific form of the transmission function: $\lambda(t) = s \times log_{10}(V(t))$. While there is some empirical support for transmission potential being related to the log-transformed viral load (mostly from studies assessing HIV transmission potential, e.g. [6, 7, 8]), other functional relationships are of course possible. For example, influenza virus transmission potential may be linearly related to viral titers or modulated by the amount of nasal discharge [20]. Onset of symptoms may also impact transmission potential since individuals experiencing symptoms may reduce their contact rates. In theory, our approach could be modified to estimate parameters of a different transmission function, with downstream analyses being analogous to those before. In practice, the transmission function we choose to estimate will always be an approximation and will in part be limited by what measurements have been taken and logged in these experimental studies. Finally, the experimental transmission study we analyzed used ferrets that were naïve to influenza infection. Clearly, cross-immunity generated from previous infection with seasonally circulating viruses could mitigate the risk of pandemic emergence of certain IAV subtypes. To consider the risk of pandemic emergence in the context of existing (cross-)immunity, experimental transmission studies could use ferrets with previous immune histories. Indeed, several transmission studies have already been performed using "pre-immune" ferrets [21] and future work could apply the approach we developed here to data from these studies.

Despite the limitations of our approach and of experimental transmission studies more generally, the method presented here advances integration of pandemic risk assessment with quantitative modeling. We suggest that our approach will be most useful for comparing the pandemic potential of different influenza viruses circulating in non-human reservoirs. Experimental transmission studies are commonly part of an overall risk assessment pipeline that characterizes multiple virological traits thought to be related to pandemic risk [22]. Our data-driven model enriches the insight that can be gained from these experiments. This should help those assessing risk to more accurately weigh pandemic potential and allocate resources appropriately.

Furthermore, we hope that quantitative modeling will become more integrated with efforts to prioritize viruses for enhanced surveillance more generally, whether through experimental challenge and transmission studies or through genetic and phenotypic characterization. A specific benefit of integrating experimental and modeling approaches

is the extension of valuable information obtained at the scale of transmission pairs to estimate parameters relevant to viral spread at the population scale. There have been calls for further synthesis of computation and modeling into influenza risk assessments for at least a decade [2], but many aspects of pandemic potential are still studied separately in wet and dry labs. Our method represents one way in which experimental and modeling approaches can be combined for improved influenza pandemic risk assessment.

Methods

Design of the experimental transmission study

Here, we analyze data from a series of experimental transmission studies in ferrets carried out in [5]. The H1N1 experimental transmission study used the IAV isolate recombinant A/California/07/2009 (H1N1pdm09). Index ferrets were inoculated at one of five inoculum doses: 10^0, 10^1, 10^2, 10^4, and 10^6 TCID_{50}. Four index ferrets were challenged at each of these five doses. Each index ferret was housed in a custom-built transmission cage with a single contact ferret. These cages are designed such that the index and contact ferret are separated by a 5 cm wide double offset perforated divider which allows animals to share the same airspace, but prevents direct physical contact. The contact ferret was introduced one day post index inoculation. Nasal washes were collected every other day from index animals beginning on day 1 post inoculation and from contact animals beginning on day 2 post inoculation (1 day post exposure, dpe). For some experiments, samples were collected up to 11 dpe; for others, samples were collected up to 13 dpe. Virus was titrated using tissue culture infectious dose assays with a limit of detection of 10^1 TCID_{50}/mL. For our analyses, the infection status of an index or contact animal was considered positive if at least one sample had a viral titer measurement that fell above the limit of detection (10^1 TCID_{50}/mL).

The H3N2 experimental transmission study used the IAV isolate recombinant A/Hong Kong/1/1968. Index ferrets were inoculated at one of six inoculum doses: 10^0, 10^1, 10^2, 10^3, 10^4, and 10^6 TCID_{50}. Four index ferrets were challenged at each of these six doses. Other components of the H3N2 study were analogous to those of the H1N1 study.

Estimation of the transmission function

We quantified the relationship between viral titer and onward transmission potential using longitudinal viral titer data from paired index-contact ferrets. To do this, we use equations developed to estimate the force of infection using the standard 'catalytic' model [23]. This model assumes that an individual is initially uninfected and susceptible to infection. With time, the individual may become exposed to the pathogen, such that the probability of testing positive increases with time. More quantitatively, the probability that an individual has been infected by time T is given by $1-e^{-\lambda T}$, where λ is a constant force of infection. This equation has been extended to allow for a time-varying force of infection (e.g., see [24]). In this case, the probability that an individual has been infected by time T is given by $Pr(-)_T = 1 - e^{-\int_0^T \lambda(t)dt}$.

We adopt this time-varying force of infection approach in our analysis of the experimental transmission studies, where the force of infection on the contact animal comes from the index animal. This force of infection is time-varying because it depends on the viral titers of the index animal and these change over time (see Figure 1). More specifically, we let the force of infection be given by equation (1). To evaluate the force of infection $\lambda(t)$ from an index ferret over the course of infection, we therefore need to know that animal's viral titers across all time points. To estimate the complete within-host viral trajectory for each index ferret, we linearly interpolated viral titers on the logarithmic scale. This assumption is equivalent to assuming exponential growth/decay kinetics between measured data points. During this fit, we assume that viral titers below the limit of detection are at the limit of detection. We further assume that the force of infection λ is 0 for all viral titers that fall at or below the limit of detection of 10^1 TCID_{50}/mL.

For each contact ferret, we determine whether the ferret has yet been infected with the focal IAV at each of its measured timepoints. Prior to the first positive viral titer measurement, the ferret is considered uninfected. On the day of the first positive viral

titer measurement, the ferret is considered infected. We use these timepoints to estimate the parameter s of the transmission function using maximum likelihood. For a contact ferret that does not become infected over the study period, we calculate for a give value of s, the probability that this contact remained uninfected by the final study timepoint (T_f). This probability is given by:

$$Pr(-)_{T_f} = e^{-\int_0^{T_f} \lambda(t)dt} \tag{2}$$

For a contact ferret that does become infected, we compute the probability that this ferret became infected between the time of its last negative test (T_1) and the time of its first positive test (T_2). This probability is given by the product of the probability that the contact has not become infected by time T_1 and the probability that the contact becomes infected between times T_1 and T_2 times:

$$Pr(+)_{T1 \to T2} = e^{-\int_0^{T_1} \lambda(t)dt} \times (1 - e^{-\int_{T_1}^{T_2} \lambda(t)dt}) \tag{3}$$

For any value of s, the overall likelihood is given by the product of the likelihoods across all contact ferrets (both those who became infected and those that did not). All but one infected index animal was used to estimate s. The one index animal (and corresponding contact animal) we excluded was from the H3N2 experiment (at a dose of 10^4 TCID_{50}/mL). We excluded this index-contact pair because the index animal was missing one viral titer measurement at 4 days post exposure.

Given a parameterized transmission function, the probabilities of infection shown in Figure 2B are calculated as:

$$Pr(+)_T = 1 - e^{-\lambda T} \tag{4}$$

where $\lambda = s \times log_{10}(V)$ and $T = 1$ day.

Quantification of parameters at the transmission event

To project the number of H1N1 secondary cases, we used the viral titer dynamics of the H1N1 infected contact animals, which we considered our population of "theoretical" index H1N1 animals. As we had done previously for the index animals when estimating the parameter s, we used linear interpolation to obtain continuous viral titer levels for each of these contact animals. We performed 1000 stochastic projections for the H1N1 virus. For each stochastic realization, we assumed each animal has l one-hour long contacts per day for the duration of their infection. (We used $l = 15$ in Figure 3 based upon previous estimates for the number of daily contacts for children [9]. We explore the impact of assuming different contact rates in Figure 4.) To simulate daily contacts for each animal, we randomly choose 15 timepoints within each day and determine the viral titer in the animal at these timepoints. With $V(t_{i,d})$ denoting the animal's viral titer for contact number i on day d, we then calculate the probability of successful transmission at each of these timepoints using equation 4, with $T = 1/24$ days and the maximum-likelihood value of s for the H1N1 virus. The total number of secondary cases from a given contact animal is then given by $\sum_d \sum_{i=1}^{l} \Psi_{i,d}$ where $\Psi_{i,d}$ denotes a random variable that is 1 with probability $Pr_{i,d}(+)$ and 0 otherwise. For each successful transmission (that is, where the random variable $\Psi_{i,d}$ is 1), we store the infection time $t_{i,d}$. This infection time corresponds to the generation interval for this transmission event, defined as the time between infection of an individual and an onward transmission. In Figure 3C, we plot the distribution of these generation intervals for all onward transmissions in the population of H1N1 infected contact animals.

We summarize across the 1000 stochastic realizations as follows. We plot in Figure 3E, the mean number of secondary infections from the population of H1N1 infected

contact animals. This mean number corresponds to the basic reproduction number R_0, and we plot the distribution of these R_0 values. To estimate the extent of transmission heterogeneity across these realizations, we follow the approach outlined in [10] and estimate the overdispersion parameter k of the negative binomial distribution for each stochastic realization using its simulated distribution of secondary cases. The overdispersion parameter is estimated using the fitdistrplus package in R [25]. We do not estimate k for the subset of stochastic realizations that do not result in any secondary cases from any of the animals. In Figure 3F we plot the cumulative distribution function of this overdispersion parameter for the subset of stochastic realizations that had at least one onward transmission. Finally, we calculate the mean generation interval T_c for each stochastic realization and plot the distribution of calculated T_c values across the 1000 simulations in Figure 3G.

Stochastic realizations for the H3N2 virus are performed in an analogous manner to those for the H1N1 virus. Summaries across the H3N2 stochastic realizations are also performed in an analogous manner. We statistically compare the R_0 and T_c estimates for the H1N1 virus and the H3N2 virus using Welch's two sample t-test.

Prediction of pandemic potential and dynamics

In Figure 4B, we show the probability of viral establishment across a range of contact rates for two different transmission heterogeneity parameterizations: one in which the overdispersion parameter $k = \infty$ (corresponding to a Poisson distribution of secondary infections across individuals) and one in which the overdispersion parameter $k = 1$ (corresponding to a geometric distribution of secondary infections across individuals). Probabilities of establishment are calculated using the probability generating function:

$$g(s) = (1 + \frac{R_0}{k}(1 - s))^{-k}$$

as described in detail in [10].

In Figure 4C, we plot the average length of a stuttering transmission chain. For contact rates that result in an $R_0 < 1$ for a virus, the average length μ of a stuttering chain is given by $\mu = \frac{1}{1-R_0}$ [26].

In Figure 4C, we plot the intrinsic growth rate r of a viral epidemic that would establish under a given contact rate. We do so by setting the mean generation time T_c for H1N1 to 4.11 days and the mean generation time T_c for H3N2 to 4.40 days. These T_c values were calculated using 1000 stochastic realizations for each virus, this time at a rate of 100 one-hour long contacts per day to ensure that mean generation times were robustly estimated. Intrinsic growth rates were then estimated under two different assumptions for the generation interval distribution: one in which the distribution is given by an exponential distribution with the mean generation time given by a virus's T_c value and one in which the distribution is given by a delta distribution with the generation time given by the virus's T_c value. In the former case, $r = \frac{R_0-1}{T_c}$ [13]. In the latter case, $r = \frac{\ln(R_0)}{T_c}$ [13].

Acknowledgements

This work was supported by the National Institute of Allergy and Infectious Diseases of the National Institutes of Health under the award numbers F31AI186550 and T32AI138952 (E.D.S.) and by the National Institute of Allergy and Infectious Diseases Centers of Excellence for Influenza Research and Response (CEIRR) contract 75N93021C00017 (K.K., T.C.S., A.C.L.). Research reported in this publication was further supported by Emory University and the Infectious Diseases Across Scales Training Program (IDASTP, E.D.S.). These studies were also supported by the by the USDA National Institute of Food and Agriculture, Hatch project 4955 (T.C.S.). The content is solely the responsibility of the authors and does not necessarily represent the official views of IDASTP, Emory University, The Pennsylvania State University, the National Institutes of Health, or the USDA.

References

[1] Lipsitch M, Barclay W, Raman R, Russell CJ, Belser JA, Cobey S, et al. Viral factors in influenza pandemic risk assessment. eLife. 2016 Nov;5:e18491. Available from: https://doi.org/10.7554/eLife.18491.

[2] Russell CA, Kasson PM, Donis RO, Riley S, Dunbar J, Rambaut A, et al. Improving pandemic influenza risk assessment. eLife. 2014 Oct;3:e03883. Publisher: eLife Sciences Publications, Ltd. Available from: https://doi.org/10.7554/eLife.03883.

[3] van Riel D, Munster VJ, de Wit E, Rimmelzwaan GF, Fouchier RAM, Osterhaus ADME, et al. Human and Avian Influenza Viruses Target Different Cells in the Lower Respiratory Tract of Humans and Other Mammals. The American Journal of Pathology. 2007 Oct;171(4):1215-23. Available from: https://www.sciencedirect.com/science/article/pii/S0002944010623851.

[4] Buhnerkempe MG, Gostic K, Park M, Ahsan P, Belser JA, Lloyd-Smith JO. Mapping influenza transmission in the ferret model to transmission in humans. eLife. 2015 Sep;4:e07969. Publisher: eLife Sciences Publications, Ltd. Available from: https://doi.org/10.7554/eLife.07969.

[5] Field CJ, Septer KM, Patel DR, Weaver VC, Sim DG, Restori KH, et al. Defining the transmissible dose 50%, the donor inoculation dose that results in airborne transmission to 50% of contacts, for two pandemic influenza viruses in ferrets. bioRxiv. 2025 Mar. Pages: 2025.03.04.641289 Section: New Results. Available from: https://www.biorxiv.org/content/10.1101/2025.03.04.641289v1.

[6] Chakraborty H, Sen PK, Helms RW, Vernazza PL, Fiscus SA, Eron JJ, et al. Viral burden in genital secretions determines male-to-female sexual transmission of HIV-1: a probabilistic empiric model. AIDS. 2001 Mar;15(5):621. Available from: https://journals.lww.com/aidsonline/fulltext/2001/03300/viral_burden_in_genital_secretions_determines.12.aspx.

[7] Quinn TC, Wawer MJ, Sewankambo N, Serwadda D, Li C, Wabwire-Mangen F, et al. Viral Load and Heterosexual Transmission of Human Immunodeficiency Virus Type 1. New England Journal of Medicine. 2000 Mar;342(13):921-9. Publisher: Massachusetts Medical Society _eprint: https://www.nejm.org/doi/pdf/10.1056/NEJM200003303421303. Available from: https://www.nejm.org/doi/full/10.1056/NEJM200003303421303.

[8] Hollingsworth TD, Anderson RM, Fraser C. HIV-1 Transmission, by Stage of Infection. The Journal of Infectious Diseases. 2008 Sep;198(5):687-93. Available from: https://doi.org/10.1086/590501.

[9] Mossong J, Hens N, Jit M, Beutels P, Auranen K, Mikolajczyk R, et al. Social Contacts and Mixing Patterns Relevant to the Spread of Infectious Diseases. PLOS Medicine. 2008 Mar;5(3):e74. Publisher: Public Library of Science. Available from: https://journals.plos.org/plosmedicine/article?id=10.1371/journal.pmed.0050074.

[10] Lloyd-Smith JO, Schreiber SJ, Kopp PE, Getz WM. Superspreading and the effect of individual variation on disease emergence. Nature. 2005 Nov;438(7066):355-9. Number: 7066 Publisher: Nature Publishing Group. Available from: https://www.nature.com/articles/nature04153.

[11] Antia R, Regoes RR, Koella JC, Bergstrom CT. The role of evolution in the emergence of infectious diseases. Nature. 2003 Dec;426(6967):658-61. Number: 6967 Publisher: Nature Publishing Group. Available from: https://www.nature.com/articles/nature02104.

[12] Koelle K, Martin MA, Antia R, Lopman B, Dean NE. The changing epidemiology of SARS-CoV-2. Science (New York, NY). 2022 Mar;375(6585):1116-21.

[13] Wallinga J, Lipsitch M. How generation intervals shape the relationship between growth rates and reproductive numbers. Proceedings of the Royal Society B: Biological Sciences. 2006 Nov;274(1609):599-604. Publisher: Royal Society. Available from: https://royalsocietypublishing.org/doi/10.1098/rspb.2006.3754.

[14] Park SW, Sun K, Abbott S, Sender R, Bar-on YM, Weitz JS, et al. Inferring the differences in incubation-period and generation-interval distributions of the Delta and Omicron variants of SARS-CoV-2. Proceedings of the National Academy of Sciences. 2023 May;120(22):e2221887120. Publisher: Proceedings of the National Academy of Sciences. Available from: https://www.pnas.org/doi/full/10.1073/pnas.2221887120.

[15] Nishiura H, Chowell G, Safan M, Castillo-Chavez C. Pros and cons of estimating the reproduction number from early epidemic growth rate of influenza A (H1N1) 2009. Theoretical Biology and Medical Modelling. 2010 Dec;7(1):1-13. Number: 1 Publisher: BioMed Central. Available from: https://tbiomed.biomedcentral.com/articles/10.1186/1742-4682-7-1.

[16] Finkelman BS, Viboud C, Koelle K, Ferrari MJ, Bharti N, Grenfell BT. Global patterns in seasonal activity of influenza A/H3N2, A/H1N1, and B from 1997 to 2005: viral coexistence and latitudinal gradients. PLoS One. 2007 Dec;2(12):e1296.

[17] Hoa LNM, Sullivan SG, Mai LQ, Khvorov A, Phuong HVM, Hang NLK, et al. Influenza A(H1N1)pdm09 But Not A(H3N2) Virus Infection Induces Durable Seroprotection: Results From the Ha Nam Cohort. The Journal of Infectious Diseases. 2022 Jul;226(1):59-69. Available from: https://doi.org/10.1093/infdis/jiaa293.

[18] Shetty N, Shephard MJ, Rockey NC, Macenczak H, Traenkner J, Danzy S, et al. Influenza virus infection and aerosol shedding kinetics in a controlled human infection model. Journal of Virology. 2024 Nov;98(12):e01612-24. Publisher: American Society for Microbiology. Available from: https://journals.asm.org/doi/10.1128/jvi.01612-24.

[19] Richard M, van den Brand JMA, Bestebroer TM, Lexmond P, de Meulder D, Fouchier RAM, et al. Influenza A viruses are transmitted via the air from the nasal respiratory epithelium of ferrets. Nature Communications. 2020 Feb;11(1):766. Publisher: Nature Publishing Group. Available from: https://www-nature-com.proxy.library.emory.edu/articles/s41467-020-14626-0.

[20] Handel A, Brown J, Stallknecht D, Rohani P. A Multi-scale Analysis of Influenza A Virus Fitness Trade-offs due to Temperature-dependent Virus Persistence. PLOS Computational Biology. 2013 Mar;9(3):e1002989. Publisher: Public Library of Science. Available from: https://journals.plos.org/ploscompbiol/article?id=10.1371/journal.pcbi.1002989.

[21] Sage VL, Jones JE, Kormuth KA, Fitzsimmons WJ, Nturibi E, Padovani GH, et al. Pre-existing heterosubtypic immunity provides a barrier to airborne transmission of influenza viruses. PLOS Pathogens. 2021 Feb;17(2):e1009273. Publisher: Public

Library of Science. Available from: https://journals.plos.org/plospathogens/article?id=10.1371/journal.ppat.1009273.

[22] Lowen AC, Baker AL, Bowman AS, García-Sastre A, Hensley SE, Lakdawala SS, et al. Pandemic risk stemming from the bovine H5N1 outbreak: an account of the knowns and unknowns. Journal of Virology. 2025 Feb;0(0):e00052-25. Publisher: American Society for Microbiology. Available from: https://journals.asm.org/doi/full/10.1128/jvi.00052-25.

[23] Muench H. Derivation of Rates from Summation Data by the Catalytic Curve. Journal of the American Statistical Association. 1934;29(185):25-38. Publisher: [American Statistical Association, Taylor & Francis, Ltd.]. Available from: https://www.jstor.org.proxy.library.emory.edu/stable/2278457.

[24] Reiner RC, Stoddard ST, Forshey BM, King AA, Ellis AM, Lloyd AL, et al. Time-varying, serotype-specific force of infection of dengue virus. Proceedings of the National Academy of Sciences of the United States of America. 2014 Jul;111(26):E2694-702.

[25] Delignette-Muller ML, Dutang C. fitdistrplus: An R Package for Fitting Distributions. Journal of Statistical Software. 2015 Mar;64:1-34. Available from: https://doi.org/10.18637/jss.v064.i04.

[26] Blumberg S, Lloyd-Smith JO. Inference of R0 and Transmission Heterogeneity from the Size Distribution of Stuttering Chains. PLoS Computational Biology. 2013 May;9(5):e1002993. Available from: https://dx.plos.org/10.1371/journal.pcbi.1002993.

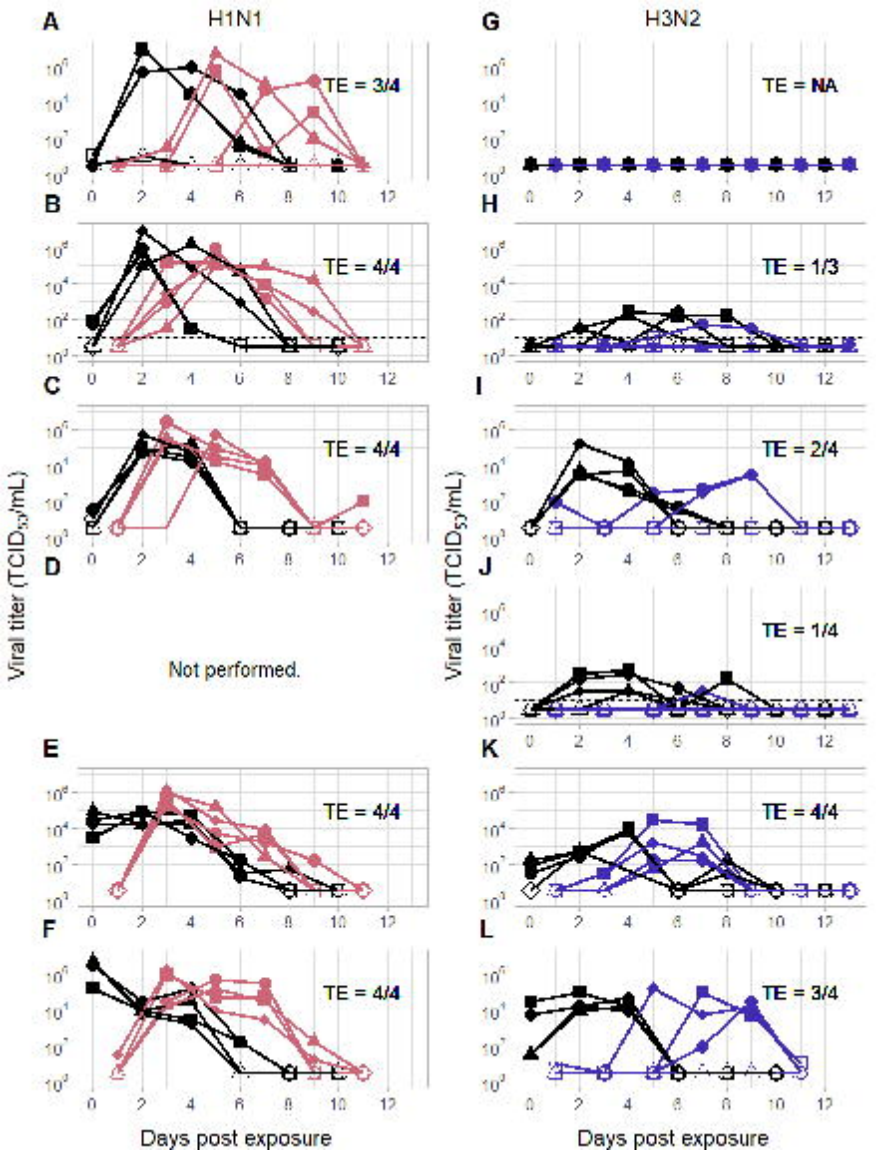
A
H1N1
TE = 3/4
B
TE = 4/4
C
TE = 4/4
D
Not performed.
E
TE = 4/4
F
TE = 4/4
G
H3N2
TE = NA
H
TE = 1/3
I
TE = 2/4
J
TE = 1/4
K
TE = 4/4
L
TE = 3/4
Viral titer (TCID50/mL)
Viral titer (TCID50/mL)
Days post exposure
Days post exposure

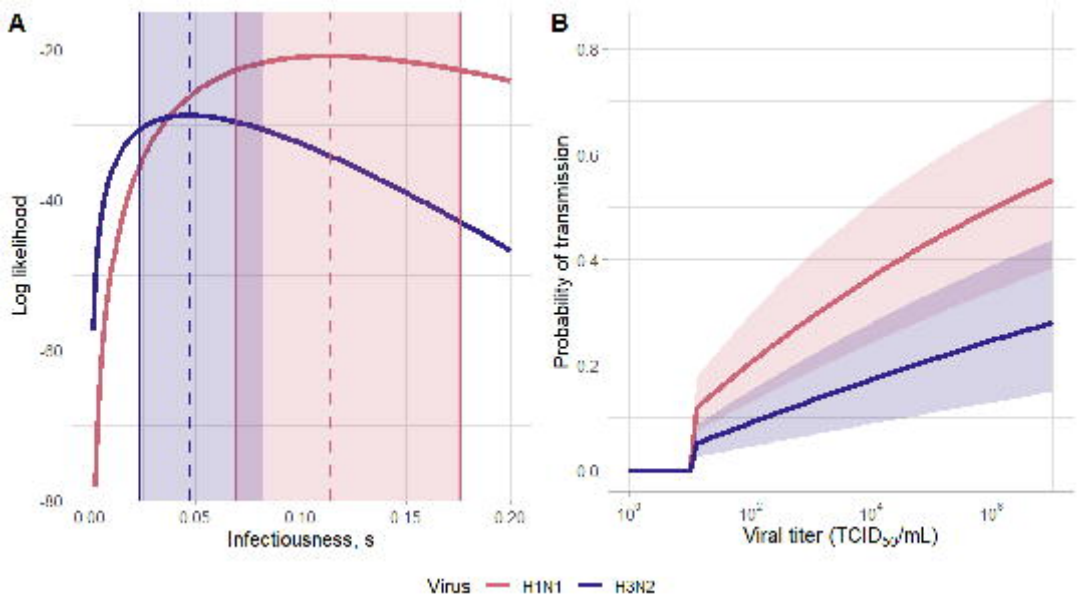
A
Log likelihood
-20
-40
-60
-80
0.00
0.05
0.10
0.15
0.20
Infectiousness, s
B
Probability of transmission
0.8
0.6
0.4
0.2
0.0
Viral titer (TCID50/mL)
Virus
H1N1
H3N2

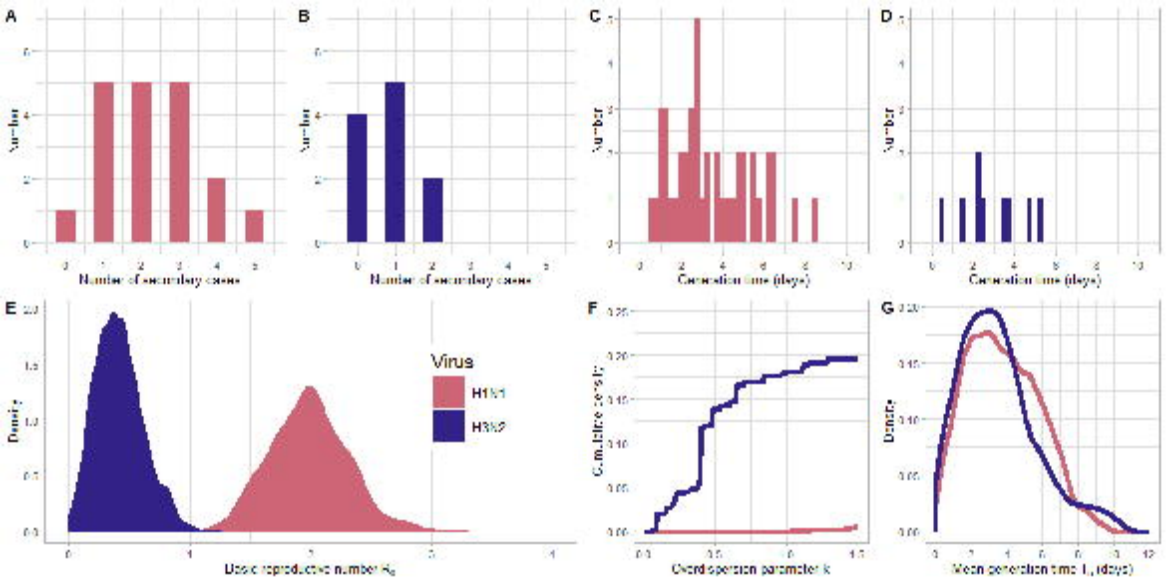
A
B
C
D
E
F
G
Number
Number of secondary cases
Generation time (days)
Density
Basic reproductive number R_0
Virus
H1N1
H3N2
Cumulative density
Overdispersion parameter k
Mean generation time T_c (days)

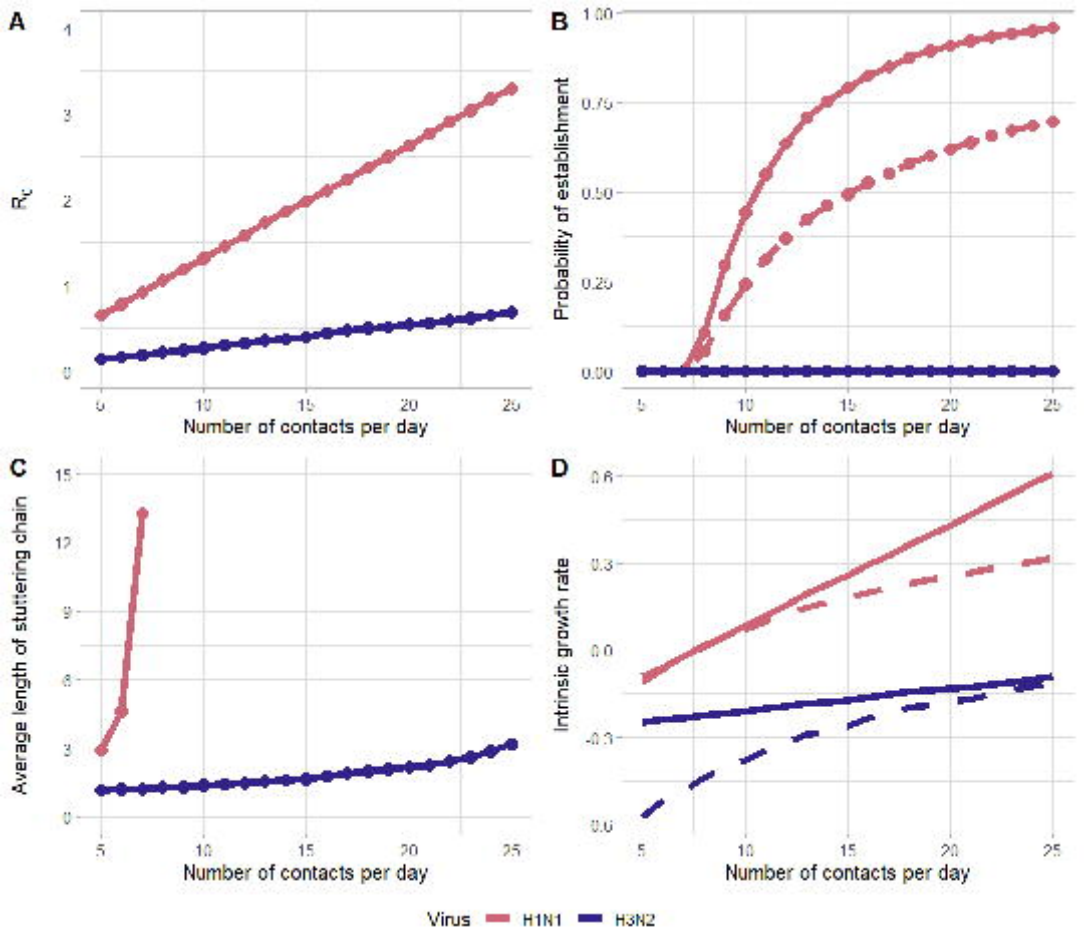
A
R_c
Number of contacts per day
B
Probability of establishment
Number of contacts per day
C
Average length of stuttering chain
Number of contacts per day
D
Intrinsic growth rate
Number of contacts per day
Virus
H1N1
H3N2